

Investigation of the effect of grain size on longitudinal critically refracted ultrasonic wave time-of-flight and velocity of propagation in material

Vikas Pralhad Dive^{1*}, Sandesh Solepatil¹, Amol Mali¹,
Sunil Dambhare¹, Aniket Kolekar¹

¹ Mechanical Engineering Department, School of Engineering, Management and Research, D. Y. Patil International University, Pune, Maharashtra, 411044, India

* Corresponding author's e-mail: vpdiv@gmail.com

ABSTRACT

This examination investigates the influence of grain size on the time-of-flight (TOF) and velocity of longitudinal critically refracted (LCR) waves in metallic materials. L_{CR} waves are pivotal in non-destructive assessment and material characterization due to their sensitivity to microstructural variations. We conducted experiments on typical varying grain sizes and analyzed the propagation of L_{CR} waves. The grain size of material changes when subjected to mechanical and thermal operations. In the present study the specimens of as received material cut to $100 \times 50 \times 8$ mm dimensions. The prepared specimens were first stress-relieved and then subjected to the heat treatments at a temperature 440 °C, 480 °C, 500 °C, 540 °C, and 560 °C for 30 minute in vacuum furnace respectively. The TOF and velocity of LCR wave were measured using an ultrasonic instrument and 5 MHz frequency transducers. The grain size and structure changes with the heat treatments, At 560 °C, and the grains became courser, and their size increased to 150 μ m. The grains get elongated at 500 °C and 540 °C, grains structure was equiaxed. The grain size of the specimens heated at 500 °C and 540 °C temperature measured as 84 μ m and 100 μ m respectively. The L_{CR} wave speed and TOF established a linear relation with grain size effect. A negative correlation was observed between LCR wave TOF and grain size. The LCR TOF is shorter for larger grain sizes and longer for smaller grain sizes. A positive correlation was observed between LCR wave speed and grain size, with rise in grain size L_{CR} wave speed increases and at lower grain size the L_{CR} wave speed observed smaller. The change in ± 10 μ m grain size changes the TOF and speed wave by ∓ 0.0005 μ sec and ± 0.2411 m/s respectively. The TOF and LCR wave velocity measurements were performed with uncertainty ± 0.000029 and ± 0.010 respectively. Our results show a significant correlation between grain size, TOF, and wave velocity, emphasizing the importance of considering grain size in ultrasonic testing and material evaluation.

Keywords: grain size, SEM, L_{CR} waves, ultrasonic techniques, time of flight, and scanning electron microscope.

INTRODUCTION

Ultrasonic examination is popularly used for non-destructive evaluation (NDE) procedures for assessing the cohesion and possessions of materials [1]. Among the various types of ultrasonic waves, L_{CR} waves are particularly useful for inspecting materials' subsurface and bulk properties. L_{CR} waves travel parallel to the surface and are highly sensitive to microstructural features such as grain size [2, 3]. This sensitivity makes

L_{CR} waves a valuable tool for characterizing material properties and detecting flaws [4]. Grain size is a critical microstructural characteristic that can change the mechanical and corporal properties of materials [5]. Previous studies have shown that grain size affects ultrasonic wave attenuation and velocity. However, there is insubstantial research with respect to outturn of grain size on L_{CR} wave TOF and speed. This study aspires to fill this breach by systematically exploring the correlation between grain size and L_{CR} wave

propagation. Grain size affects ultrasonic wave propagation through scattering and absorption mechanisms. Larger grains cause more significant scattering, which can increase attenuation and affect wave velocity [6–8]. Studies by Kolsky and Papadakis have established foundational theories on the interaction between grain boundaries and ultrasonic waves [9, 10]. More recent research has focused on quantifying these effects and developing models to predict wave behavior based on microstructural characteristics. Grain size significantly changes the mechanical and corporal properties of polycrystalline materials. Smaller grains generally enhance material strength and hardness, as outlined by the Hall-Petch relationship. Conversely, larger grains can lead to rise in spread and attenuation of ultrasonic waves, affecting their propagation characteristics.

L_{CR} waves are particularly effective for detecting subsurface defects and characterizing material properties due to their sensitivity to variations in microstructure [11]. Research by Rose and Scalea has demonstrated the utility of L_{CR} waves in various NDE applications, including the detection of stress corrosion cracking and evaluation of residual stresses [12, 13].

L_{CR} waves are widely used in NDT due to their ability to travel long distances along the surface and detect subsurface flaws. Their sensitivity to changes in material properties makes them an ideal tool for characterizing microstructural features, such as grain size. Previous studies have shown that variations in grain size can affect the TOF and speed of L_{CR} waves, but a comprehensive understanding of these effects remains incomplete. Generally, the two types of ultrasonic transducer arrangements, first L_{CR} wave and second shear wave in birefringence mode used to measure the TOF or velocity of ultrasonic wave [14–16]. The stress field direction and the ultrasonic wave's travel direction are essential in residual stress evaluation. The L_{CR} wave is a longitudinal ultrasonic wave that progresses equidistant to the surface, explicitly traveling underneath the surface at an actual depth. Hence, the L_{CR} wave termed by another name surface skimming longitudinal waves. The properties of the L_{CR} wave explained in the earlier research work [17–20].

The angle of incidence at nearly same to the first critical angle [21] determined with the help of Snell's law used to electrify the L_{CR} wave beneath the surface of the test material. Snell's law reveals that the angle of incidence and refraction

at a contact surface of two materials equals a particular wave's incident and refracted velocity ratio. Figure 1a shows the propagation of waves from one material to another with the angle of incidence and refraction.

The longitudinal wave (L) incident with a speed C_1 in the first material (PMMA) at an angle of incidence θ_1 at the contact of the second material (AA7075-T651). When an ultrasonic wave moves from low-impedance material to high-impedance material, an angle of incidence at which the refracted wave travels at an angle equivalent to 90° that angle of incidence is named as the first critical angle. As a result, the refracted wave, named as L_{CR} wave, propagates alongside the material surface.

The expression for Snell's law represented with Equation 1 and applied to calculate the first critical angle of incidence.

$$\frac{C_1}{\sin \theta_1} = \frac{C_2}{\sin \theta_2} \quad (1)$$

where: C_1 and C_2 – longitudinal wave speed in low and high impedance material, respectively ($C_2 > C_1$); θ_1 – angle of incidence, θ_2 – angle of Refraction ($\theta_2 = 90^\circ$).

METHODOLOGY AND EXPERIMENTATION

Materials

The material grade AA7075-T651 of aluminum alloy used in the current research work.

Cutting of material samples

Waterjet machining used to cut the AA7075-T651 sheets of size $100 \times 50 \times 8$ mm from as received material. Waterjet machining doesn't induce residual stresses after material cutting. Total ten plates cut to size $100 \times 50 \times 8$ mm using waterjet machining. The waterjet machined sample shown in Figure 1b. The cut material samples were inspected for the cutting dimensions.

Stress relieving of material

The specimen prepared to $100 \times 50 \times 8$ mm size and was subjected to stress relieving before the testing. The stress relieving carried out to remove the earlier built-in stresses in the components at the time of the metal manufacturing and

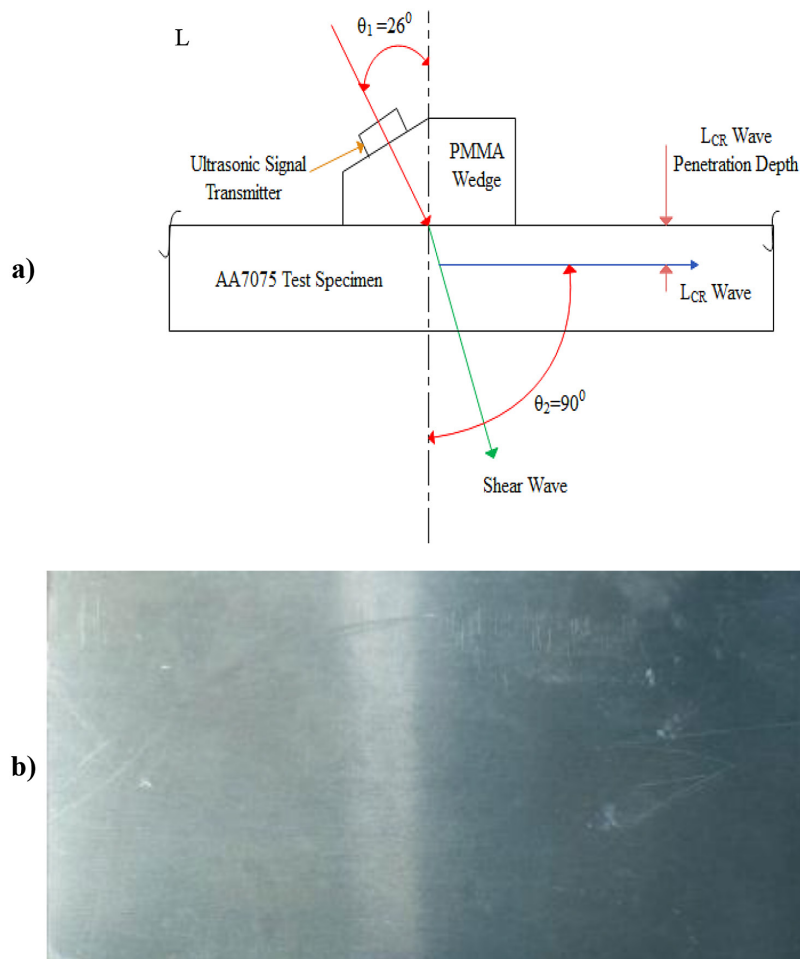


Figure 1. (a) Single L_{CR} transducer with PMMA wedge [22], (b) waterjet machined AA 7075-T651 specimen $100 \times 50 \times 8$ mm

sample preparation. The stress relieving process was carried out using a vacuum furnace. The cycle time was 120 min, and the furnace temperature was continued to be 120 °C. The ultrasonic LCR wave velocity was measured in both as-received and stress-relieved specimens.

Instrumentation for measurement of TOF and speed of ultrasonic L_{CR} wave

The ultrasonic equipment includes the ultrasonic integrated pulser/receiver, ultrasonic transducers of 10 mm diameter and 5 MHz frequency, computer with the integrated software interface, PMMA wedge, couplant, Pneumatic piston arrangement to apply pressure on ultrasonic wedge assembly.

Ultrasonic waveform generator

The ultrasonic waveform generator make of Optel OPBOX 2.1, an integrated pulser/receiver.

The pulser/receiver enabled with two signal inputs, pulse-echo (PE) and through-thickness (TT) measurement. The pulser/receiver operates at various ranges of sampling frequencies such as 5 MHz, 12 MHz, 25 MHz, 50 MHz, and 100 MHz with a resolution better than 1ns for precise measurement of the TOF of ultrasonic wave. Furthermore, the Optel OPBOX 2.1 ultrasonic box is suitable for all ultrasonic measurements because of the internal processor's many digital inputs/outputs and synchronization with the pulse signal.

Ultrasonic transducers

The main element of the ultrasonic transducer is the piezoelectric ceramic element. The piezoelectric ceramic element generates a piezoelectric effect during measurement. Ultrasonic transducers were used as both signal transmitters and receivers pulse-echo (PE) and through-thickness (TT) measurement mode. The diameter of the transducer piezoelectric element was 10 mm.

Integrated software interface

The national instrument software interfaced with the Optel OPBOX 2.1, an integrated pulser/receiver. The interface used to apply the measurement conditions and to measure the TOF and velocity of the L_{CR} ultrasonic wave. The software interface applies the inputs to do the measurements, such as pulse voltage, pulse width, sampling frequency, source selection, filter selection, and signal gain.

Wedge

The one-piece wedge of PMMA acrylic material machined with a computerized milling machine. The wedge designed on the principle of Snell's law to generate the longitudinally critical refracted (L_{CR}) ultrasonic wave. The ultrasonic wave speed in PPMA and AA7075 materials determined with the pulse-echo procedure as 2780 m/s and 6332 m/s, respectively. The ultrasonic wedge was designed with an incidence angle (first critical angle) equivalent to 26° . The PMMA material has a low acoustic impedance. The more significant difference in acoustic impedance at the boundary of the wedge and test material helps in more excellent energy reflection at the boundary of the wedge and test material.

Couplant

The contact type ultrasonic measurement was conducted with the application of semi-solid (gel type material) between the wedge and test material surface. Couplant fills the clearance space between the two contacting areas and helps to get more transmission of ultrasonic waves in the test material. Generally, carbogel, honey, oil, glycerin, and water are used as couplant during ultrasonic contact testing.

Experimentation to explore the effect of the grain size

The L_{CR} wave technique applied to estimate the built-in stresses in metallic materials. The variation in grain structure and grain size of material affects the utilization of L_{CR} wave to evaluate in-situ residual stress measurement. The current study performed to explore the out-turn of grain size on the L_{CR} wave TOF and speed in AA7075-T651 material. The different grain structures with variations in grain size obtained by applying different heat treatments [23-27].

The metallographic analysis performed to rate the grain size of the material as per ASTM E112 standards. The TOF and speed of the L_{CR} wave measured in heat treated samples [28-34]. The following steps performed to find the effect of grain size on L_{CR} wave TOF and speed:

1. Preparation of test specimen: the material machined to the required dimensions of $100 \times 50 \times 8$ mm. The stress relieving performed to remove the initial built-in stresses with the heat treatment. The material surface cleaned to remove the contamination with acetone and a steel brush. The as-received, stress-free, and heat treated samples used for further experimentation.
2. Heat treatment: the stress-relieved AA 7075 five samples kept in a vacuum furnace for 30 minutes and held at a temperature 440°C , 480°C , 500°C , 540°C , and 560°C , respectively.
3. Experiment conducted: the series of experiments performed with the application of L_{CR} wave to measure TOF and speed. The grain size of the microstructure measured with optical microscopy.
4. Analysis of data: the obtained data from the experiment analyzed to identify the trends or patterns in the L_{CR} wave TOF and speed as a function of grain size. Obtained data fitted to a mathematical model using statistical analysis to identify the correlation.

The experiments were conducted to measure the TOF and velocity of the LCR wave in AA7075 specimens as shown in Figure 2a and 2b. The couplant, applied to the test surface, fills the gap between the wedge and the test surface, ensuring maximum energy transmission of the LCR wave. Initially, the TOF and speed of the L_{CR} wave measured in stress-relieved AA7075 test material and then on heat treated specimen (1) measured with the ultrasonic transducer transmitting (7) and receiving (8) transducer mounted on PMMA wedge (6) designed based on the principle of Snell's law, to maintain the surface contact between test material and PMMA wedge couplant gel introduced, the transducers were connected at transmitting (2) and receiving (3) to an integrated pulser/receiver model: Optel OPBOX 2.1 (4) interfaced with the software (5) integrated with the DAQ, the tight contact between the wedge and test surface maintained with force applied by a pneumatic plunger (9). The five samples of waveforms were recorded and analyzed for every selected specimen. The

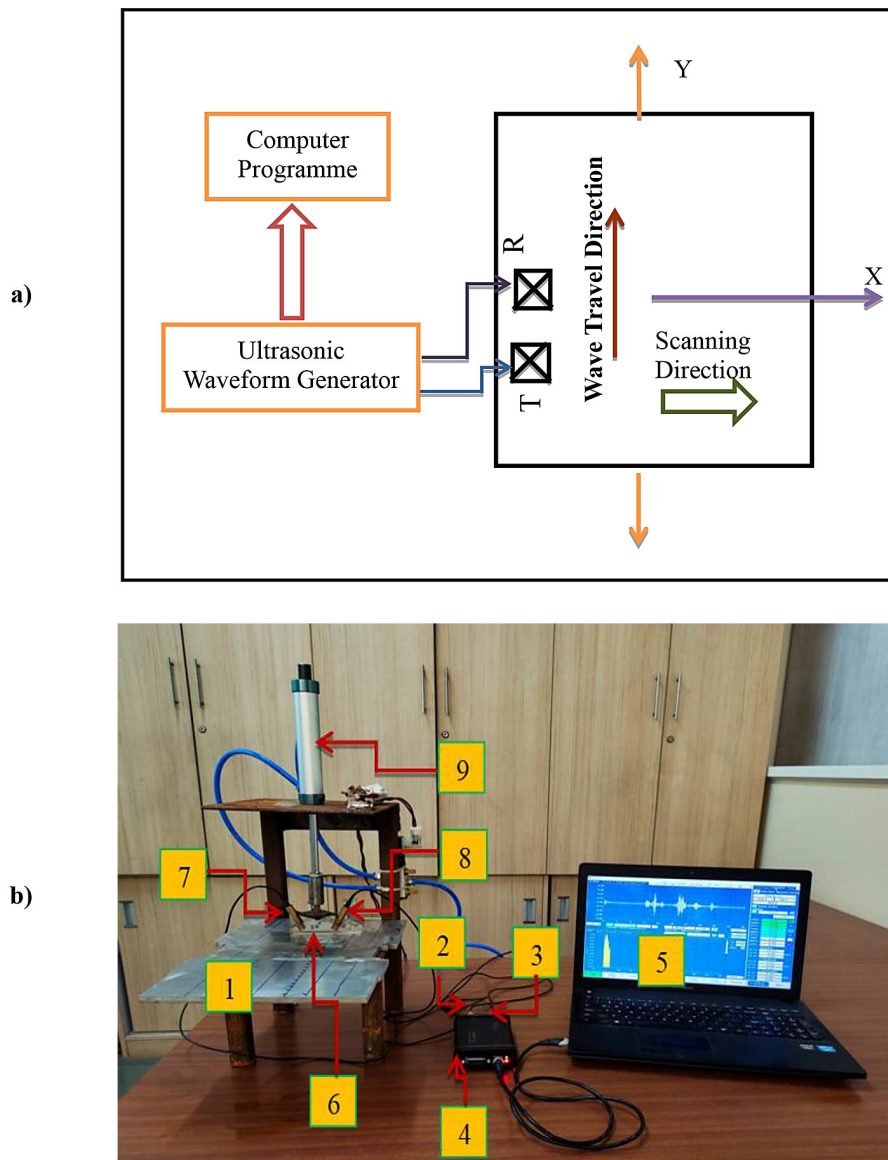


Figure 2. TOF and velocity measurement (a) diagrammatic view (b) experimental setup

ultrasonic waveform was generated using an integrated pulser/receiver Optel model OPBOX 2.01, with sampling frequency 100 MHz interfaced with a data acquisition system designed with NI 18.0 temporary LABVIEW program. The transmitting and receiving transducers with 5 MHz frequency performed the through-thickness measurements. The measurements performed at five different locations along the length to cover the specimen's complete length. The wedge allowed to move along the transverse direction at an interval of 10 mm quantify the L_{CR} wave TOF and speed in specimens. The L_{CR} wave TOF recorded thrice at each point, and the average value determined for the respective location.

The samples to study the microstructure and grain size measurements cut from the

stress-relieved, stress-free, and heat treated samples. The molds of specimens prepared, and the polishing performed to obtain a mirror finish before microstructure analysis. The polishing machine with different grades of girth paper and diamond paste of 3 μm , 1 μm particle size applied to prepare samples for metallography. Keller's etchant 10 ml HF, 5 ml HCL, 5 ml HNO_3 , and 380 ml H_2O_2 applied on the specimen surface for 35 seconds to open the grains of material in the microstructure and SEM study. All seven samples grain size was measured with Nikon Eclipse LV150NL optical microscope. The data obtained for grain size and L_{CR} wave TOF and speed plotted, and statistical analysis done to identify the correlation between grain size and L_{CR} wave TOF and speed.

EXPERIMENTAL RESULTS AND DISCUSSION

A sequence of experiments was performed to find the grain size effect on L_{CR} ultrasonic wave TOF and speed. The grain structure of AA7075-T651 as-received, stress-relieved, and heat treated specimens revealed with an optical microscope at 10X resolution shown in Figure 3. The grain size of AA7075-T651 as received, stress-relieved, and heat treated specimens measured for microstructure images as per the ASTM E112 standards with the intercept method. The Figure 3 a, and b indicate an initial grain size distribution with small, equiaxed grains. As the heat treatment temperature increases, the grains coarsen, becoming more elongated and defined in the Figures 3c, 3d, 3e, 3f, and g micrographs respectively. The Figures 3c, 3d, 3e, 3f, and 3g display significantly larger and elongated grains, consistent with recrystallization and grain growth mechanisms. The “As Received” and “Stress Relieved” samples display finer grains. The stress-relieved sample at 22 °C shows the smallest grain size 10.5 μm , suggesting that stress relief helps refine the microstructure by reducing internal strains without causing significant grain coarsening. The microstructure of Figure 3a reveals irregularly shaped grains with both equiaxed and elongated morphologies, suggesting a polycrystalline structure. Some grains appear deformed, indicating possible cold working or directional solidification. Well-defined grain boundaries suggest limited grain growth. Dark inclusions, likely oxides, are randomly distributed, with some aligning along grain boundaries due to impurity segregation. Their moderate density indicates controlled processing. The contrast variations hint at possible phase differences. The material exhibits a refined grain structure with inclusions that could affect mechanical properties such as strength and toughness. The microstructure for Figure 3b shows polygonal grains with a mix of equiaxed and elongated shapes, likely due to stress relieving process. The presence of banded structures suggests anisotropic grain growth. Well-defined grain boundaries indicate proper etching. Numerous dark inclusions, MgZn_2 and Al_2Cu . The MgZn_2 related to the GP zone formation, are distributed throughout, with a higher concentration along grain boundaries, suggesting impurity segregation. The increased inclusion density compared to the as received material may result from different processing conditions. These

inclusions can impact the material’s toughness and machinability.

The microstructure of as-received AA 7075 aluminum alloy shown in Figure 3a primarily consists of an α -Al matrix with intermetallic compounds and inclusions. Secondary phases such as MgZn_2 (η -phase), Al_2CuMg (S-phase), and Fe-rich compounds are present, particularly along grain boundaries. These phases influence mechanical properties and corrosion resistance. Dark spots in the micrograph indicate oxide inclusions of Al_2O_3 as well as Fe-based intermetallics from processing. The grain boundaries exhibit precipitate accumulation, which can lead to stress corrosion cracking (SCC) and embrittlement. In this condition, the alloy has not yet undergone significant precipitation hardening, meaning solute-rich phases dominate rather than finely distributed strengthening precipitates. The presence of intermetallic phases and grain boundary precipitates highlights the alloy’s susceptibility to environmental degradation, necessitating further processing to improve durability. The microstructure of stress-relieved AA 7075 aluminum alloy shown in Figure 3b consists of a primary aluminum matrix (α -Al) with strengthening precipitates such as MgZn_2 (η -phase) and Al_2CuMg (S-phase). These phases enhance strength through precipitation hardening. Dark contrast regions indicate Fe and Si based intermetallics inclusions. The grain boundaries exhibit morphological changes due to stress relief, reducing residual stress and refining precipitate distribution. Some inclusions, such as $\text{Al}_7\text{Cu}_2\text{Fe}$, may act as stress concentrators. The microstructure of AA 7075 aluminum alloy at 400 °C shown in Figure 4c reveals significant phase transformations. The primary α -Al matrix is present, with coarsened MgZn_2 (η -phase) precipitates along grain boundaries due to over-aging. Fe and Si-rich inclusions, such as $\text{Al}_7\text{Cu}_2\text{Fe}$, are scattered throughout. Grain coarsening occurs due to recrystallization, while prolonged exposure may lead to partial melting of low-melting eutectic phases, weakening the structure. The dissolution of fine-strengthening η' precipitates reduces mechanical strength.

The heating at 400 °C temperature causes morphological changes, precipitate coarsening, and grain boundary weakening, negatively impacting the alloy’s strength and hardness. At 480 °C, the microstructure of AA 7075 aluminum alloy shown in Figure 3d undergoes significant transformations, including phase dissolution, grain coarsening, and

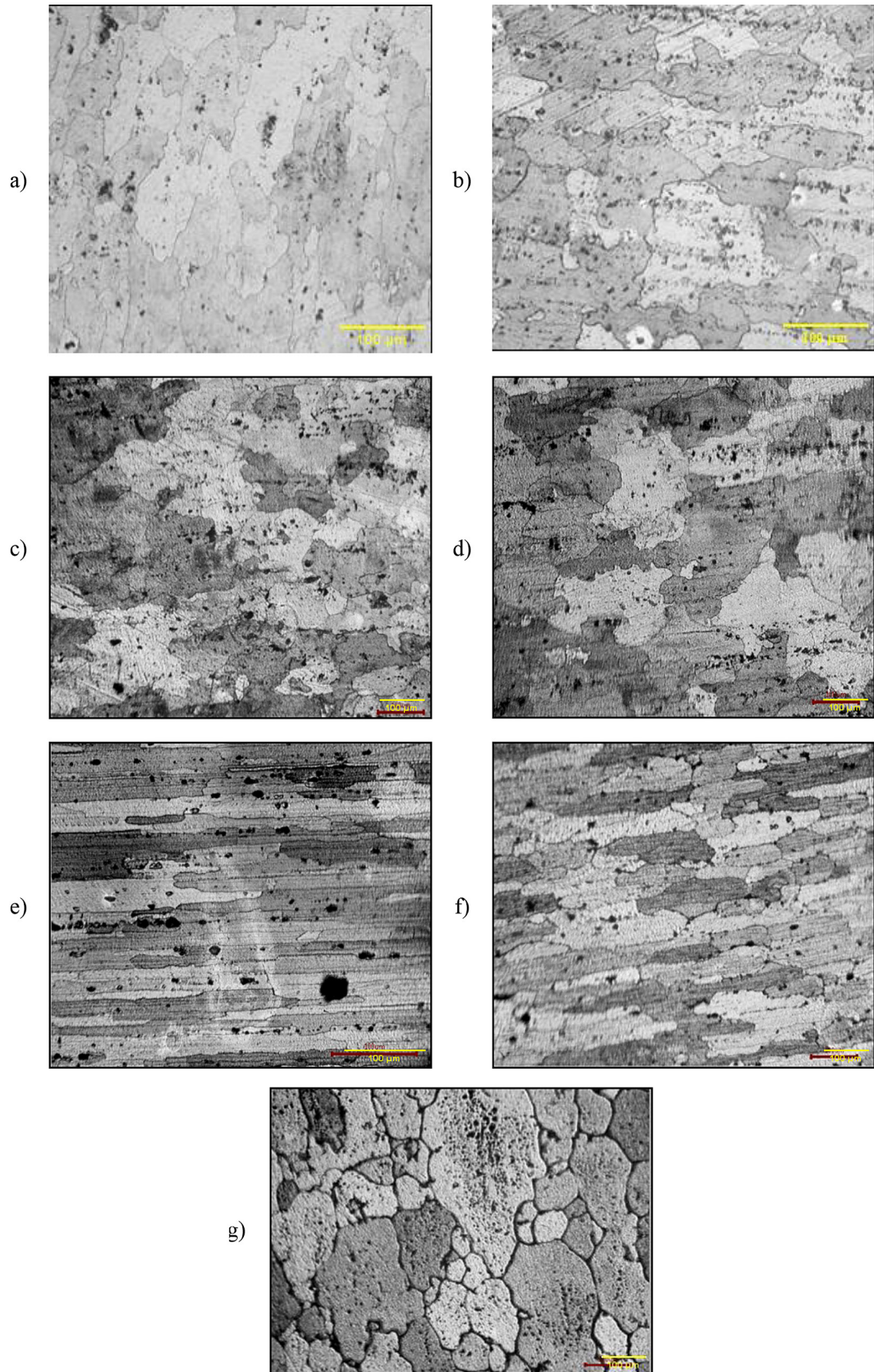


Figure 3. Microstructure captured at 10X for an AA7075-T651 (a) as received, (b) stress relieved, (c) 400 °C, (d) 480 °C, (e) 500 °C, (f) 540 °C, and (g) 560 °C

the formation of inclusions. The primary α -Al matrix remains dominant, while the η ($MgZn_2$) phase and Al-Cu-based phases appeared at grain boundaries due to high-temperature exposure. Dark spots in the microstructure suggest the presence of inclusions such as Al_2O_3 oxides and Fe-rich intermetallics, which can negatively impact alloy performance. Morphological changes include grain growth, reducing grain boundary density, and the possible occurrence of grain boundary liquation if the temperature nears the eutectic melting point. The development of precipitate-free zones (PFZs) near grain boundaries weakens localized areas. These changes collectively influence the alloy's mechanical strength, corrosion resistance, and high-temperature stability. At 500 °C, AA 7075 aluminum alloy undergoes significant microstructural and mechanical degradation as shown in Figure 3 (e). The primary strengthening phases, such as $MgZn_2$ (η phase) and Al_2CuMg (S phase), begin to dissolve and coarsen, reducing the alloy's strength. Grain boundary liquation occurs due to the partial melting of low-melting phases, leading to intergranular cracking and embrittlement. Additionally, oxidation and inclusion formation, such as Al_2O_3 and Mg-based oxides, further deteriorate mechanical properties. These microstructural changes cause a notable drop in tensile strength, hardness, and fracture toughness while increasing the risk of creep deformation and hot cracking.

The microstructure of AA 7075 aluminum alloy shown in Figure 3f at 540 °C primarily consists of an α -aluminum matrix with dispersed intermetallic phases like η ($MgZn_2$) and Fe or Si-based inclusions. At this temperature, grain coarsening occurs due to recrystallization, while $MgZn_2$ dissolves, reducing strengthening effects. Small dark inclusions, Fe-rich phases, are visible. Grain boundary changes include precipitate-free zones (PFZs) and potential liquation, weakening mechanical properties. The microstructure of AA

7075 aluminum alloy shown in Figure 3g at 560 °C exhibits significant phase transformations and morphological changes. The primary α -Al matrix appears as the light gray regions, while second-phase precipitates such as $MgZn_2$ (η phase) and Al_3Fe may be present, undergoing partial dissolution or coarsening. Eutectic structures can also form due to localized melting along grain boundaries. Inclusions such as oxide particles (Al_2O_3) and iron-rich intermetallic phases (Al-Fe-Si) are likely present, appearing as darker regions. Additionally, porosity or voids observed due to partial melting and resolidification. Morphologically, the high temperature promotes grain growth through recrystallization, leading to a coarser structure. Grain boundary weakening is evident due to liquid phase formation, which can reduce mechanical strength and increase susceptibility to hot cracking. The presence of second-phase particles along grain boundaries may further act as stress concentrators, leading to structural instability. These microstructural changes indicate that the alloy has been subjected to high thermal exposure, affecting its mechanical properties. The grain size and the grain structure changes with the heat treatments.

At 560 °C temperature, the grains became coarser, and the size of the grains increased to 150 μm . The grains get elongated at 500 °C and at 540 °C temperature grains structure observed approaching to equiaxed nature. The grain size of the specimens heated at 500 °C and 540 °C temperatures measured as 84 μm and 100 μm , respectively. The grain sizes of the samples ranged from 10 μm to 150 μm , with a uniform distribution across the sample surfaces. The heat treatment processes were effective in producing the desired grain sizes, as confirmed by optical microscopy.

The L_{CR} wave TOF and speed measured with ultrasonic instruments. The outcome of the measurements condensed in Table 1.

Table 1. Grain size and L_{CR} wave TOF, speed in AA7075-T651 heat treated, as received and stress-relieved specimens

Heat treatment temperature (°C)	Average grain size (μm)	L_{CR} wave speed (m/s)	L_{CR} wave TOF (μsec)
440	32	6530	12.25
480	49	6534	12.24
500	84	6542	12.22
540	100	6548	12.21
560	150	6558	12.19
As received	12.5	6425	12.45
Stress relieved sample @ 22 °C	10.5	6364	12.57

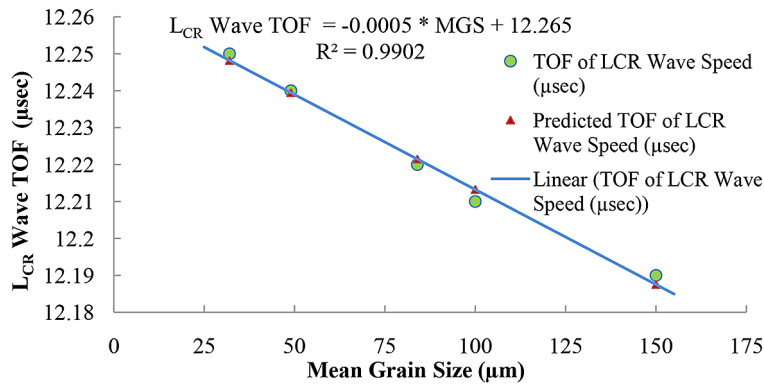


Figure 4. TOF of L_{CR} wave in AA7075-T651 with respect to grain size

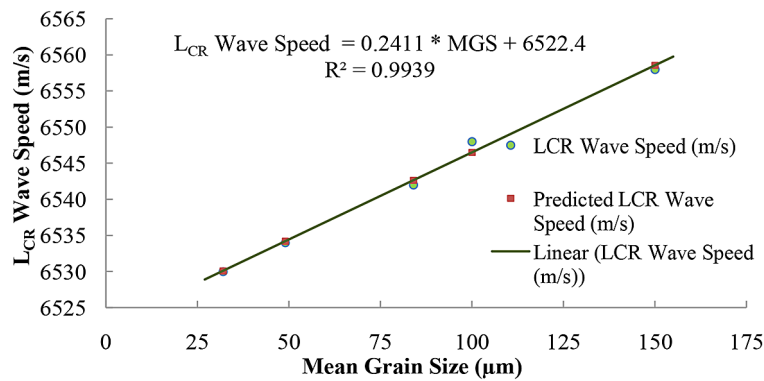


Figure 5. Speed of L_{CR} wave in AA7075-T651 with respect to grain size

Figure 4 and 5 shows the variation in L_{CR} wave TOF and speed with change in grain size, respectively. The 240 grains per grain size sample across five different grain sizes was analyzed to find the effect of grain size on LCR wave TOF and speed. The grain size determined with a standard deviation error of 4.042 μm . The structural heterogeneity was observed in the result due to mixing of fine and coarse grains with varying deformation and recrystallization. The results showed a clear correlation between grain size and L_{CR} wave TOF and speed. Samples with larger grain sizes exhibited longer TOF and lower wave speeds compared to samples with smaller grain sizes. The relationship was quantified using linear regression analysis, revealing a statistically significant dependence of TOF and wave speed on grain size. The data points closely follow the linear trend, confirming that Mean Grain Size significantly influences TOF. The L_{CR} wave speed and TOF established a linear relation with the grain size effect. The L_{CR} ultrasonic wave TOF and grain size fixed negative relation; the L_{CR} TOF decreased at larger grain sizes and increased at smaller grain sizes

confirming that larger grains allow faster wave transmission. $R^2 = 0.9902$ suggests a very strong linear relationship between the two variables, meaning the data fits the trend line extremely well. Green circles represent the actual TOF of LCR Wave Speed. Red triangles represent the Predicted TOF of LCR Wave Speed. A blue line represents the linear trend. The slope -0.0005 suggests that for each unit increase in grain size 10 μm , the TOF decreases by 0.0005 μsec . Conversely, the L_{CR} wave speed and grain size established positive relation; with an increase in grain size, the L_{CR} wave speed increases, and at a decrease in grain size, the L_{CR} wave speed decreases due to reduced scattering effects in coarser microstructures.

$R^2 = 0.9939$ suggests a very strong linear relationship between the two variables, meaning the data fits the trend line extremely well. Green circles represent the actual speed of LCR Wave. Red rectangles represent the Predicted speed of LCR Wave. A black line represents the linear trend. The slope $+0.2411$ m/s suggests that for each unit increase in grain size 10 μm , the wave speed increases by 0.2411 m/s.

The change in $\pm 10 \mu\text{m}$ grain size changes the TOF and speed of the L_{CR} wave by $\mp 0.0005 \mu\text{s}$ and $\pm 0.2411 \text{ m/s}$, respectively. The TOF and speed of the L_{CR} wave measurements performed with uncertainty ± 0.000029 and ± 0.010 , respectively.

CONCLUSIONS

The study systematically examines as-received, stress-relieved, and heat-treated samples, filling the gap in understanding how stress relief and grain growth affect LCR wave properties. This investigation has demonstrated a significant turnout of grain size on L_{CR} wave TOF and speed. The findings highlight the importance of considering grain size in ultrasonic testing and material characterization. Future research should focus on developing comprehensive models that account grain size effects and exploring the application of LCR waves in various industrial contexts. The heat treatment experiments at $440 \text{ }^\circ\text{C}$ to $560 \text{ }^\circ\text{C}$ introduce controlled grain growth, allowing a detailed analysis of LCR wave interaction with different microstructures. The methodology enhances wave penetration and minimizes unwanted mode conversions, improving measurement accuracy. The L_{CR} wave speed and TOF established a linear function with the grain size effect. The L_{CR} ultrasonic wave TOF and grain size fixed negative relation; the L_{CR} TOF less at larger grain size and higher at smaller grain size. On the other hand, the L_{CR} wave speed and grain size established positive relation; with the rise in grain size, the L_{CR} wave speed increases, and at smaller grain size, the L_{CR} wave speed observed to be smaller. The observed increase in TOF and decrease in wave speed with larger grain sizes were responsible to the increased spreading and attenuation of L_{CR} waves at grain boundaries. Larger grains create more substantial barriers to wave propagation, leading to longer travel times and reduced velocities. These findings are consistent with the theoretical predictions and previous studies on ultrasonic wave behavior in polycrystalline materials. Understanding the effect of grain size on LCR wave propagation is crucial for refining the precision and reliability of ultrasonic testing. By accounting for grain size variations, NDE practitioners can enhance defect detection and material characterization. The novel linear equations derived can be used for predicting grain size

based on ultrasonic measurements, contributing to real-time microstructure evaluation in industry. The findings are directly applicable in aerospace, automotive, and manufacturing industries where AA7075-T651 is widely used. The study provides valuable insights that can be used to develop more accurate models and calibration techniques for ultrasonic testing. Any material processing alters material characteristics, potentially leading to misinterpretation of measurement results. In this study, the characterization of the material above the critical temperature of the material studied. The study guides material characterizations by applying the L_{CR} wave ultrasonic nondestructive method.

Acknowledgement

I sincerely appreciate the guidance and support of Mr. Harjit Singh, Scientist/Engineer-SF, Mechanical Design and Analysis Entity, Liquid Propulsion Systems Centre, Valiamala, Trivandrum. I am also deeply grateful to Dr. Shaligram, Director of the ISRO-UoP Space Technology Cell at Savitribai Phule Pune University, Ganeshkhind, Pune, for his invaluable assistance. Additionally, I extend my heartfelt thanks to Dr. Mrs. A.V. Patil, Director of the School of Engineering, Management, and Research, as well as Prof. Prabhat Ranjan, Vice Chancellor of D.Y. Patil International University, Pune, for providing the necessary resources and a conducive research environment.

This research is conducted under the ISRO-UoP Joint Research Programme, Ref. No.: PU/ISRO-STC/1944, dated 05/07/2018.

REFERENCES

1. Hirsekorn S. The scattering of ultrasonic waves by polycrystals. *The Journal of the Acoustical Society of America*, 1982; 72(3), 1021–1031. <https://doi.org/10.1121/1.388233>
2. Dive V., Lakade S. Characterization of ultrasonic LCR wave penetration in materials with finite element simulation. *AIP Conf. Proc.* 21 March 2024; 3013(1): 020011. <https://doi.org/10.1063/5.0202059>
3. Palanichamy P., Joseph A., Jayakumar T., Raj B. Ultrasonic velocity measurements for estimation of grain size in austenitic stainless steel, *NDT & E International*. 1995; 28(3), 179–185. [https://doi.org/10.1016/0963-8695\(95\)00011-L](https://doi.org/10.1016/0963-8695(95)00011-L)
4. Hull J.B., Langton C.M., Barker S., Jones A.R.

- Identification and characterisation of materials by broadband ultrasonic attenuation analysis, *Journal of Materials Processing Technology*, 1996; 56(1–4), 148–157. [https://doi.org/10.1016/0924-0136\(96\)85100-4](https://doi.org/10.1016/0924-0136(96)85100-4)
5. Vikas D., Lakade S. Microstructure and microhardness investigation of non-weldable AA7075-T651 alloy with gas tungsten arc welding, *International review of Mechanical Engineering*, 2022; 6(16), 265–276. <https://doi.org/10.15866/ireme.v16i6.21905>
 6. Ahn B., Lee S.S., Hong S.T., Kim, H.C., Kang S.J.L. Application of the acoustic resonance method to evaluate the grain size of low carbon steels, *NDT & E International*, 1999; 32(2), 85–89.
 7. Botvina L.R., Fradkin L.J., Bridge B. A new method for assessing the mean grain size of polycrystalline materials using ultrasonic NDE, *Journal of materials science*, 2000; 35, 4673–4683. <https://doi.org/10.1023/A:1004890604013>
 8. Walaszek H., Hoblos J., Bourse G., Robin C. Effect of microstructure on ultrasonic measurements of residual stresses in welded joints, *Material Science Forum*, 2002; 404–407, 875–880. [10.4028/www.scientific.net/msf.404-407.875](https://doi.org/10.4028/www.scientific.net/msf.404-407.875)
 9. Kolsky H. The propagation of stress waves in solids, *Journal of Sound and Vibration*, 1966; 1(1), 88–110. [https://doi.org/10.1016/0022-460X\(64\)90008-2](https://doi.org/10.1016/0022-460X(64)90008-2)
 10. Papadakis, E. P. Ultrasonic attenuation caused by scattering in polycrystalline metals, *Journal of Applied Physics*, 36(9), 2595–2600, <https://doi.org/10.1121/1.1909401>
 11. Vikas D., Sanjay L. Recent research progress on residual stress measurement using non-destructive testing, *Materials Today: Proceedings*, 2021; 47(11), 3282–3287. <https://doi.org/10.1016/j.matpr.2021.07.094>
 12. Rose J.L. *Ultrasonic Waves in Solid Media*. Cambridge University Press, 1999.
 13. Scalea F.L. Ultrasonic guided waves for nondestructive testing, *Journal of Nondestructive Evaluation*, 2004; 23(3), 123–134.
 14. Ahn B., Lee S.S. Effect of microstructure of low carbon steels on ultrasonic attenuation. *IEEE transactions on ultrasonic, ferroelectrics, and frequency control*, 2000; 47(3), 620–629. <https://doi.org/10.1109/58.842049>
 15. Choi S., Ryu J., Kim J.S., Jhang K.Y. Comparison of linear and nonlinear ultrasonic parameters in characterizing grain size and mechanical properties of 304L stainless steel, *Metals*, 2019; 9(12), 1279, <https://doi.org/10.3390/met9121279>
 16. Wan T., Naoe T., Wakui T., Futakawa M., Obayashi H., Sasa T. Effects of grain size on ultrasonic attenuation in type 316L stainless steel, *Materials*, 2017; 10(7), 753, <https://doi.org/10.3390/ma10070753>
 17. Brekhovskikh L. *Waves in Layered Media*, 2nd edition, Academic press, New York, 1976.
 18. Basatskaya L.V. and Ermolov I.N. Theoretical analysis of ultrasonic longitudinal undersurface waves in solid medium, *Sov. J. Nondestruct. Test*, 1981; 16(7), 524–530.
 19. Junghans P. and Bray D.E. Beam characteristics of high angle longitudinal wave probes, in *NDE: Applications, Advanced Methods, and Codes and Standards*, R.N. Pangbom, D.E. Bray, J.F. Cook, C.D. Colwfer, and D.M. Schlader, Eds., vol. 216 of PVP, vol. 9 of NDE of Proceedings of the Pressure Vessels and Piping Conference, San Diego, California, 1991, [https://doi.org/10.1016/0963-8695\(92\)90366-O](https://doi.org/10.1016/0963-8695(92)90366-O)
 20. Langenberg, K.J., Fellenger, P., Marklein, R. On the nature of the so-called subsurface longitudinal wave and/or the surface longitudinal ‘creeping’ wave, *Res. Nondestructive Evaluation*, 2, 1990; 59–81. <https://doi.org/10.1007/BF01606421>
 21. Dickens J.R., Bender D.A., Bray D.E. A critical-angle ultrasonic technique for the inspection of wood parallel to grain”, *Wood and Fiber Science*, 1996; 45–47.
 22. Bray D.E., Tang W. Subsurface stress evaluation in steel plates and bars using the L_{CR} ultrasonic wave, *Nuclear Engineering and Design*, 2001; 207, 231–240. [https://doi.org/10.1016/S0029-5493\(01\)00334-X](https://doi.org/10.1016/S0029-5493(01)00334-X)
 23. Qozam H., Hoblos J., Bourse G., Robin C., Walaszek H., Bouteille P., Cherfaout M. Ultrasonic stress measurement in welded component by using L_{CR} waves: Analysis of the microstructure effect, *Material Science Forum*, 2006; 524–525, 453–458.
 24. Sarpun I., Kilickaya M., Tuncel S. Mean grain size determination in marbles by ultrasonic velocity techniques, *NDT & E International*, 2005; 38(1), 21–25, <https://doi.org/10.1016/j.ndeint.2004.06.009>
 25. Aghaie-Khafri M., Honarvar F., Zanganeh S. Characterization of grain size and yield strength in AISI 301 stainless steel using ultrasonic attenuation measurements, *Journal of Nondestructive Evaluation*, 2012; 31, 191–196. <https://doi.org/10.1007/s10921-012-0134-z>
 26. Ahn B., Lee S.S., Hong S.T., Kim, H.C., Kang S.J.L. Application of the acoustic resonance method to evaluate the grain size of low carbon steels, *NDT & E International*, 1999; 32(2), 85–89.
 27. Ahn B., Lee S.S. Effect of microstructure of low carbon steels on ultrasonic attenuation *IEEE transactions on ultrasonic, ferroelectrics, and frequency control*, 2000; 47(3), 620–629.
 28. Liu B., Miao W., Dong S., He P. Grain size effect on L_{cr} elastic wave for surface stress measurement of carbon steel, *Nondestructive Testing and Evaluation*, 2018; 33(2), 139–153.

29. Liu B., Miao W., Dong S. He P. Grain size correction of welding residual stress measurement in a carbon steel plate using the critical refraction of longitudinal waves, *Research in Nondestructive Evaluation*, 2019; 30(2), 112–126, <https://doi.org/10.1080/09349847.2017.1375170>
30. Bouda A.B., Lebaili S., Benchaala A. Grain size influence on ultrasonic velocities and attenuation, *NDT & E International*, 2003, 36(1), 1–5, [https://doi.org/10.1016/S0963-8695\(02\)00043-9](https://doi.org/10.1016/S0963-8695(02)00043-9)
31. Buenos A.A., dos Santos Jr. A.A., Pereira Jr. P., Santos C.S. Effect of mean grain size in the time of flight for L_{cr} Waves, In *ASME International Mechanical Engineering Congress and Exposition American Society of Mechanical Engineers*, 2012; 45264, 63–69. <https://doi.org/10.1115/IMECE2012-89055>
32. Buenos A.A., Pereira Jr. P., Mei P.R., dos Santos A.A. Influence of grain size on the propagation of L_{CR} waves in low carbon steel, *Journal of Nondestructive Evaluation*, 2014; 33(4), 562–570, <https://doi.org/10.1007/s10921-014-0252-x>
33. Qozam H., Chaki S., Bourse G., Robin C., Walaszek C., Bouteille P. Microstructure effect on the L_{cr} elastic wave for welding residual stress measurement, *Experimental Mechanics*, 2010; 50, 179–185, <https://doi.org/10.1007/s11340-009-9283-0>
34. Babu S.A.V., Giridharan, P.K., Ramesh Narayanan, P., & Murty N. Microstructural investigations on ATIG and FBTIG welding of AA 2219 T87 aluminum alloy, *Applied Mechanics and Materials*, 2014; 592, 489–493.